Coalescence of Elastic Blisters Filled with a Viscous Fluid

Torstein Sæter,[1] Christian Pedersen,[1,‡] Jacco H. Snoeijer,[2] Thomas Salez,[3,*] and Andreas Carlson[1,†]

[1]*Department of Mathematics, Mechanics Division, University of Oslo, Oslo 0316, Norway*
[2]*Physics of Fluids Group, Faculty of Science and Technology, University of Twente, 7500 AE Enschede, The Netherlands*
[3]*Univ. Bordeaux, CNRS, LOMA, UMR 5798, F-33400 Talence, France*

Pockets of viscous fluid coalescing beneath an elastic sheet are encountered in a wide range of natural phenomena and engineering processes, spanning across scales. As the pockets merge, a bridge is formed with a height increasing as the sheet relaxes. We study the spatiotemporal dynamics of such an elastohydrodynamic coalescence process by combining experiments, lubrication theory, and numerical simulations. The bridge height exhibits an exponential growth with time, which corresponds to a self-similar solution of the bending-driven thin-film equation. We address this unique self-similarity and the self-similar shape of the bridge, both of which are corroborated in numerical simulations and experiments.

Viscous flows beneath an elastic sheet hold significant relevance in various natural phenomena and industrial processes. Examples include flow-driven intrusions of elastic fronts [1–8], viscous adhesion of elastic sheets and cell membranes [9,10], soft viscous fingering instabilities [11–13], as well as in geological processes such as sill or laccolith formation [14–16].

When two fluid pockets are trapped between an elastic sheet and a prewetted solid substrate, forming what we refer to as blisters, they will spread and eventually merge if they are in close proximity. As they meet, the elastic bending of the sheet will, at short times, relax the system into a single blister that, at long times, flattens by spreading [2,17]. This situation is analogous to the extensively studied phenomenon of capillary-driven drop coalescence, where different flow regimes [18–21] and the effect of liquid rheology [22,23] have been characterized. Hernández-Sánchez *et al.* [21] demonstrated that the bridge connecting two coalescing viscous sessile droplets grows linearly with time, which was described by a similarity solution of the governing lubrication model. Recently, also the self-similar form for the three-dimensional bridge shape has been derived [24]. Despite the prevalence of elastohydrodynamic coalescence, a comprehensive understanding of the underlying physical processes involved is currently lacking. This Letter addresses this knowledge gap by employing a combination of experiments, lubrication theory, and numerical simulations. We reveal that the short-time asymptotic relaxation dynamics can be described by a universal self-similar solution with an anomalous exponential growth with time, contrasting the power-law solutions usually describing the self-similar behavior of lubrication flows, and we quantify the details of the spatiotemporal dynamics.

We consider an elastic sheet that is separated from the solid substrate by a thin liquid film of height $\tilde{h}_\infty$, as shown in Fig. 1. Two identical pockets, forming the blisters, are generated by the influx of viscous liquid through two inlets (diameters 4×10^{-3} m) at the supporting substrate, separated by a distance $2R_0 = 0.15$ m. After a given volume is injected, the pump is turned off allowing the blisters to spread until they make contact. We define $\tilde{t} = 0$ as the time the blisters make contact, with the height of the blister peak $\tilde{h}_i$. The system is designed to have $\tilde{h}_i/d < 1$, where d is the plate thickness, and $\tilde{h}_i/R_0 \ll 1$. The cross-sectional height profile $\tilde{h}(\tilde{x}, \tilde{y} = 0, \tilde{t})$ of the fluid film is obtained by passing a laser line along the $\tilde{x}$ coordinate through the blister peaks. A Nikon camera captures images of the laser line every 2 s, at an angle of 25° relative to the horizontal plane. The measured laser line is fitted with a Gaussian intensity distribution along each vertical column of pixels. This imaging setup allows for the visualization and measurement of the height profile with time.

The circular elastic sheet of diameter $D = 0.4$ m and thickness $d = 5.7 \times 10^{-3}$ m is made from a silicon-based elastomer (Zhermack, Elite Double), with Young's modulus $E = 0.25$ MPa and Poisson ratio $\nu = 0.5$ [25], giving a bending stiffness $B = Ed^3/[12(1-\nu^2)] = 5 \times 10^{-3}$ N m. Different silicone oils, with viscosities $\mu \in [0.1, 0.35, 0.5]$ Pa s, and density $\rho = 970$ kg m^{-3} are used as fluids. The supporting rigid plexiglass substrate and the bottom side of the flat elastic sheet are both precoated with oil using a squeegee, before gently put in contact. A fluid film of thickness $\tilde{h}_\infty = (40 \pm 14) \times 10^{-6}$ m hence separates the two flat solids before any fluid injection through the inlets. $\tilde{h}_\infty$ is determined on a smaller plate ($21 \times 24 \times 10^{-4}$ m^2) by weighing it with and without the prewetted film, with an error estimate determined from 40 repetitions. Air bubbles trapped underneath the elastic sheet are visually identified through the transparent substrate. These bubbles are removed by
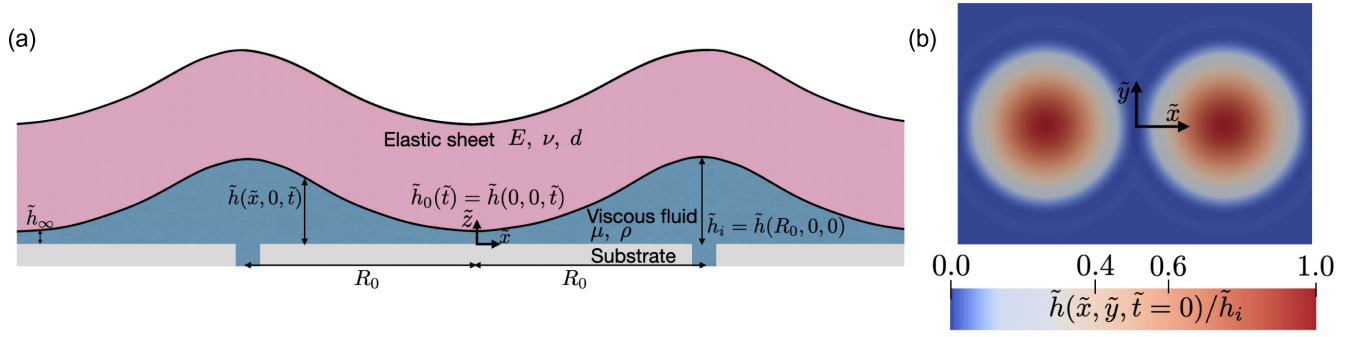
(a)

(b)

FIG. 1.   (a) Schematic ($\tilde{y} = 0$) of the studied system. Two identical pockets filled with a viscous fluid of viscosity μ and density ρ are created by injecting prescribed fluid volumes beneath an elastic sheet. The elastic sheet has a Young's modulus E, a Poisson ratio ν, and a thickness d. After the fluid injection is stopped, each blister spreads until reaching a radius R_0 when they meet, which is defined as time $\tilde{t} = 0$. The fluid height profile is $\tilde{h}(\tilde{x}, \tilde{y}, \tilde{t})$, while $\tilde{h}_0(\tilde{t}) = \tilde{h}(0, 0, \tilde{t})$ is the bridge height, $\tilde{h}_i = \tilde{h}(\pm R_0, 0, 0)$ is the initial blister height, and $\tilde{r}(\tilde{t})$ is the half-width of the bridge along the $\tilde{y}$ axis (into the plane). (b) Contour plot of the nondimensional height profile $\tilde{h}(\tilde{x}, \tilde{y}, \tilde{t})/\tilde{h}_i$ from the three-dimensional simulation when the two blisters make contact ($\tilde{t} = 0$).

carefully squeezing the elastic sheet in the corresponding regions, transporting the bubbles to the edge whereas the sheet has time to relax before liquid is injected at the inlets.

After injecting a prescribed fluid volume with a Merck-Millipore-Sigma syringe pump, the two blisters spread until they make contact. The experimental determination of the contact point is partly limited by our spatial resolution of 0.067 mm/pixel, leading to an uncertainty in defining the contact time $\tilde{t} = 0$ [further discussed in Supplemental Material (SM) [26]]. It is also worth noting that the experiments have a mean asymmetry of $6.3 \pm 4.7\%$ between the two blisters peaks at the defined moment of contact. This grade of asymmetry is shown numerically to have negligible impact on the results (see SM [26]). We define $\tilde{h}_i$ as the average between the two blister heights at $\tilde{t} = 0$. Varying the injected fluid volume, we obtain $\tilde{h}_i \in [1.9$–$4.2] \times 10^{-3}$ m (for more information, see SM [26]).

We use the elastohydrodynamic lubrication theory [1,27–29] to rationalize the experimental measurements. Assuming no-slip at the two solid boundaries, conservation of mass, and an incompressible Newtonian lubrication flow, the fluid height profile $\tilde{h}(\tilde{x}, \tilde{y}, \tilde{t})$ satisfies the thin-film equation. By nondimensionalizing the variables with $x = \tilde{x}/R_0$, $y = \tilde{y}/R_0$, $h(x, y, t) = \tilde{h}(\tilde{x}, \tilde{y}, \tilde{t})/\tilde{h}_i$, $h_\infty = \tilde{h}_\infty/\tilde{h}_i$, and $t = \tilde{t}/T$ with $T = \mu R_0^6/(B\tilde{h}_i^3)$, we obtain

$$\frac{\partial h(x, y, t)}{\partial t} = \frac{1}{12} \nabla \cdot [h^3(x, y, t) \nabla p(x, y, t)], \quad (1)$$

$$p(x, y, t) = \nabla^4 h(x, y, t) + N h(x, y, t), \quad (2)$$

where $\nabla = [(\partial/\partial x), (\partial/\partial y)]$ is the nabla operator. $p(x, y, t)$ is the excess hydrodynamic pressure generated by elastic bending of the plate and gravity, neglecting any effect from stretching the plate as the edge is free to move and $\tilde{h}_i < d$ [5,8]. In Eq. (1) a single nondimensional number

$N = \rho g R_0^4/B = (R_0/L_e)^4$ appears, which is the ratio between gravity and elastic bending, i.e., an elastic equivalent of the Bond number. Here, g is the gravitational acceleration and $L_e = [B/(\rho g)]^{1/4}$ is the elastogravity length. By inserting our material properties from the experiments we obtain $L_e = 28 \times 10^{-3}$ m $= 0.36 R_0$, and $N \approx 59$.

Equations (1) and (2) are solved numerically by using a finite-element method. We discretize the equations using linear elements and use an implicit-time marching scheme [5]. At $t^* = 0$, the simulations are initialized with two identical bumps centered at $(x, y) = (\pm 1, 0)$, as

$$h(x, y, t^* = 0) = h_\infty + 0.6[(1 - \{[(x \pm 1)^2 + y^2]/0.75^2\})^2]$$

for $\sqrt{(x \pm 1)^2 + y^2} \leq 0.75$, $h(x, y, t^* = 0) = h_\infty$ otherwise. After a few time steps, the height profile becomes smooth and the two blisters spread a short distance before they make contact. We set the moment of contact as the new temporal origin $t = 0$, defined as the first time step in the simulations where the bridge height $h_0(t) \geq h_\infty$, followed by a monotonic growth of $h_0(t)$. Thereafter, we rescale the profile so that $h(\pm 1, 0, 0) = 1$. To reduce the computational time, we only simulate a quarter of each blister due to symmetry, and therefore apply the symmetry conditions at all the boundaries: $\nabla h(x, y, t) \cdot \mathbf{n} = \nabla^3 h(x, y, t) \cdot \mathbf{n} = \nabla^5 h(x, y, t) \cdot \mathbf{n} = 0$ with $\mathbf{n}$ the normal vector to the boundary. We use a nonuniform grid, which is refined around the bridge with minimum mesh size $\Delta x = 1.25 \times 10^{-4}$, and an adaptive time stepping routine with maximum time step $\Delta t = 1.6 \times 10^{-4}$.

We now turn our attention to the coalescence dynamics, after the blisters have made contact. An example of the temporal evolution of the height profiles is illustrated in Fig. 2(a). The numerical solutions and the experiments are in close agreement. The thickness $\tilde{h}_\infty = 40 \times 10^{-6}$ m of the prewetted layer together with the peak height $\tilde{h}_i = 2.55 \times 10^{-3}$ m, obtained from the experiments give
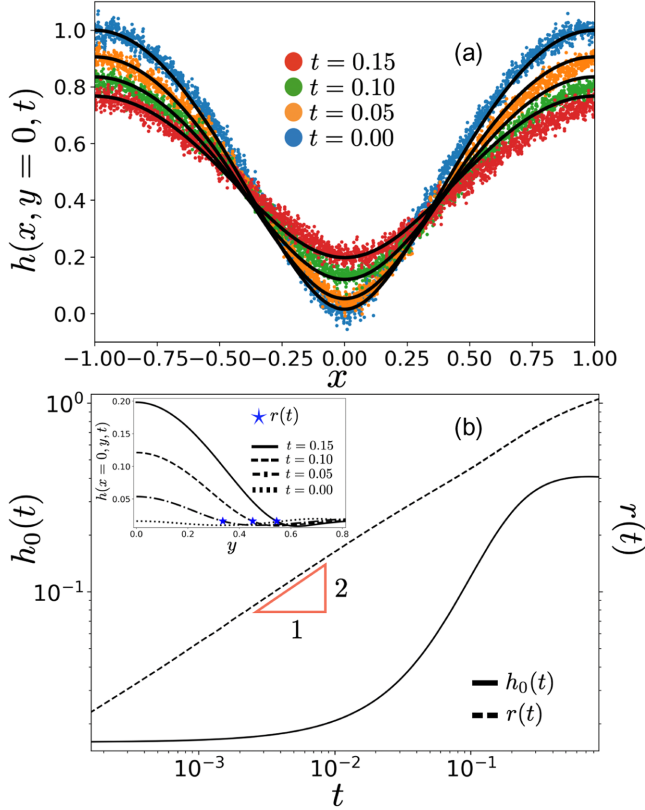
FIG. 2. (a) Nondimensional cross-sectional height profiles $h(x, y = 0, t)$, at different nondimensional times t, from an experiment with $\mu = 0.5$ Pa s and $\tilde{h}_i = 2.55$ mm, and from the numerical solutions (solid lines) of Eq. (1) with $N = 59$ and $h_\infty = 0.016$. (b) Nondimensional height $h_0(t)$, and half-width $r(t)$ of the bridge, extracted from the numerical solutions of Eq. (1). Inset: The two-dimensional bridge profile along the y axis, $h(x = 0, y, t)$ at the same nondimensional times as in (a). $r(t)$ is extracted numerically as the first point along y where $h(x = 0, y > 0, t) \le h_\infty$, indicated with a star marker.

$h_\infty = 0.016$, which is the same as the value used in the numerical simulation. From the numerical height profiles, we extract the bridge half-width $r(t)$ and height $h_0(t) = h(0, 0, t)$, as shown in Fig. 2(b). The inset shows the two-dimensional bridge profile along the y axis, $h(x = 0, y, t)$, at the same nondimensional time instants as in Fig. 2(a). The half-width is defined as the first point along y where $h(x = 0, y > 0, t) \le h_\infty$. It is striking to observe that these two quantities $[r(t), h_0(t)]$ have very different behavior with time: the half-width follows a power law $r(t) \sim t^{1/2}$, which is reminiscent to the capillary case [20], while the bridge height $h_0(t)$ clearly deviates from a power law behavior.

To understand the bridge height dynamics, we take inspiration from the self-similar analysis of the elastohydrodynamic blister growth [2], and from the capillary coalescence case [20,21]. We assume that the flow is predominantly oriented along the x direction, so that we can consider a two-dimensional problem. At the small

scales associated with the initial stages of coalescence, the dynamics are driven by elastic bending and gravity can be neglected. Therefore, Eq. (1) simplifies to

$$\frac{\partial h(x, t)}{\partial t} = \frac{1}{12} \frac{\partial}{\partial x}\left[h^3(x, t)\frac{\partial^5 h(x, t)}{\partial x^5}\right], \tag{3}$$

where $h(x, t)$ is the two-dimensional height profile of the bridge. Let us look for a similarity solution $H(\xi) = h(x, t)/f(t)$ of Eq. (3), with $\xi = x/g(t)$, where $f(t)$ and $g(t)$ are two unknown functions [30]. At short times, we consider the quasistatic shape of the blister [2] as a constant outer solution for the coalescence dynamics, instead of the interface slope (or contact angle) used for the capillary case [21]. The quasistatic blister shape has a nonzero nondimensional "contact curvature" κ [2]. We set $[\partial^2 h(x, t)/\partial x^2]|_{x\to\infty} = \kappa$, which, by inserting the postulated self-similar formulation for the bridge profile, can be written

$$\frac{f(t)}{g^2(t)} H''(\infty) = \kappa. \tag{4}$$

For the case without gravity ($N = 0$), the contact curvature follows from the blister shape at constant bending pressure [2], which in the present units gives $\kappa_0 = 8$. For the case with gravity ($N = 59$), the contact curvature $\kappa = 8.8$ is found to be slightly larger (see SM [26] for more information). For convenience, and without loss of generality, we normalize the similarity solution such that $H''(\infty) = 1$, from which it follows that $f(t) = \kappa g^2(t)$. Inserting the similarity variable transform into Eq. (3), we obtain

$$\frac{1}{\kappa^3} \frac{\dot{g}(t)}{g(t)} = \alpha = \frac{1}{12} \frac{\left[H(\xi)^3 H'''''(\xi)\right]'}{2H(\xi) - \xi H'(\xi)}, \tag{5}$$

where the dot and prime indicate derivatives with respect to t and ξ, respectively. Owing to the separation of variables, the parameter α must be a constant that needs to be determined. We thus obtain two ordinary differential equations (ODEs). The solution of the ODE for $g(t)$ reads

$$g(t) = g(0) \exp(\beta t), \quad \text{with} \quad \beta = \alpha \kappa^3. \tag{6}$$

As a consequence, one gets $f(t) = \kappa g(0)^2 \exp(2\beta t)$. To the best of our knowledge, this is the first time that an anomalous exponential self-similar solution is derived for the thin-film equation, in contrast to conventional power laws typically describing the self-similar behavior of lubrication flows. Exponential self-similar solutions have, however, been found in other physical phenomena, e.g., in diffusion dynamics [30,31].
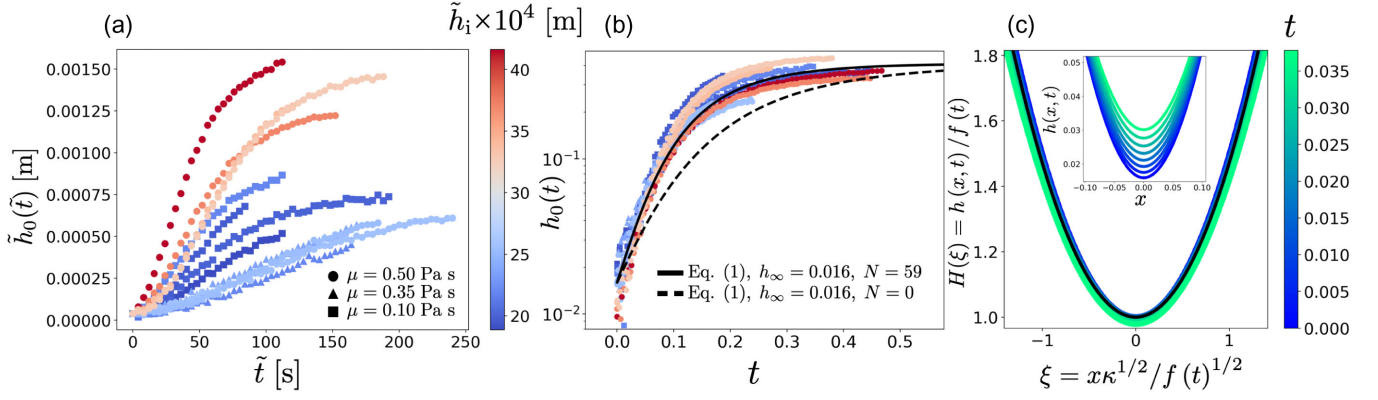
FIG. 3. (a) Experimental bridge height $\tilde{h}_0(\tilde{t})$ for different viscosities $\mu \in [0.1, 0.35, 0.5]$ Pa s and blister peak heights $\tilde{h}_i \in [1.9 - 4.2] \times 10^{-3}$ m. (b) Experimental nondimensional bridge height $h_0(t) = \tilde{h}_0(t)/\tilde{h}_i$ as a function of nondimensional time $t = \tilde{t}/T$. The solid and dashed lines represent the numerical solutions of Eq. (1) for $N = 59$ and $N = 0$, respectively, and with $h_\infty = 0.016$. The short-time behavior for $N = 59$ is well described by $h_0(t) = h_0(0) \exp(26t)$; while for $N = 0$ it follows $h_0(t) = h_0(0) \exp(17.9t)$. (c) Inset: the bridge height profiles $h(x, y = 0, t)$ [denoted as $h(x, t)$] from the short-time numerical solution of Eq. (1) for $N = 0$ and $h_\infty = 0.016$. Main: self-similar representation of the height profiles ($y = 0$) from Eq. (1) ($N = 0$) shown in the inset. Here, we used $f(t) = 0.016 \exp(17.9t)$ and $\kappa = 8$. The black solid line is the numerical solution of Eq. (5) with $\kappa = 8$ and $\alpha = 0.0175$.

We proceed to test the prediction from Eq. (6) by using the experimental and numerical data. The experimental data of the temporal evolution of the bridge height $\tilde{h}_0(\tilde{t})$, for $\tilde{h}_i \in [1.9 - 4.2] \times 10^{-3}$ m and $\mu \in [0.1, 0.35, 0.5]$ Pa s, is shown in Fig. 3(a). It is clear that both μ and $\tilde{h}_i$ affect the relaxation dynamics. As expected, increasing the viscosity slows down the dynamics. The effect of $\tilde{h}_i$ is more subtle, but consistent with the prediction for a dimensional growth rate $\tilde{\beta} = \tilde{\alpha}\tilde{\kappa}^3$, where $\tilde{\kappa}$ is the dimensional contact curvature and $\tilde{\alpha}$ is a constant. A larger $\tilde{h}_i$ increases the contact curvature of the blisters ($\tilde{\kappa} \sim \tilde{h}_i/R_0^2$), thereby enhancing the growth rate. In Fig. 3(b), the same data are recast into nondimensional form that collapses it onto a nearly single curve. The numerical solution of Eq. (1) with $N = 59$ reproduces the dynamics measured in the experiments, which at short times corresponds to an exponential growth with $\beta = 13.00$. For comparison, the numerical solution of Eq. (1) with $N = 0$ is also shown, which at short times has a $\beta_0 = 8.95$. Assuming that α is independent of N, one gets that β/β_0 is given by $(\kappa/\kappa_0)^3$, as observed within a $\sim 9\%$ margin of error. The error is likely stemming from uncertainties in the exponential fits and in the extracted values for κ and κ_0. However, α does depend on the nondimensional prewetted layer thickness h_∞, where a smaller h_∞ leads to a smaller exponential growth rate (see SM [26]). Therefore, α is not a universal constant, and equals $\alpha = \beta_0/\kappa_0^3 \approx 0.0175$ in our case.

Finally, we investigate the self-similarity of the bridge profile $H(\xi)$ through Eq. (5). The latter is a sixth-order nonlinear ODE, which is solved for $\alpha = 0.0175$, using the numerical solver *bvp5c* in MATLAB with boundary conditions: $H'(0) = H'''(0) = H'''''(0) = 0$, $H''(\infty) = 1$, and

$H'''(\infty) = H''''(\infty) = 0$. Since the bridge is symmetric around $\xi = 0$ and has a constant far-field curvature it provides the required six boundary conditions, so we do not impose $H(0) = 1$ in contrast to the capillary case [21]. Nevertheless, by introducing the rescaled variables $\xi^* = \xi/H(0)^{1/2}$ and $H^*(\xi^*) = H(\xi)/H(0)$, one can always enforce $H^*(0) = 1$, without having it explicitly stated in the boundary conditions. The results for the self-similar profile are shown in Fig. 3(c). The close agreement between the numerical solution of Eq. (5) and the numerical solution of Eq. (1) for $N = 0$ manifests that the shape of the bridge is described by the self-similar profile found from Eq. (5), and corroborate the validity of the similarity solution.

In this Letter, we have demonstrated that, as two pockets of viscous fluids merge under an elastic sheet, the connecting bridge has a height that grows exponentially with time. The spatiotemporal dynamics agree between the experiments and the numerical solutions of the thin-film equation. Moreover, a self-similar exponential solution is found, which rationalizes the short-time dynamics found in the experiments and numerical simulations. To the best of our knowledge, this represents the first exponential self-similar solution for lubrication flows, standing in sharp contrast to the conventional power-law solutions. Our finding highlights the significant and nontrivial role played by the interaction between elastic deformations and viscous lubrication flows.

---

[*]thomas.salez@cnrs.fr

[†]acarlson@math.uio.no

[‡]Present address: Expert Analytics, Møllergata 8, 0179 Oslo, Norway.

[1] A. E. Hosoi and L. Mahadevan, Phys. Rev. Lett. **93,** 137802 (2004).

[2] J. R. Lister, G. G. Peng, and J. A. Neufeld, Phys. Rev. Lett. **111,** 154501 (2013).

[3] I. J. Hewitt, N. J. Balmforth, and J. R. De Bruyn, Eur. J. Appl. Math. **26,** 1 (2015).

[4] T. V. Ball and J. A. Neufeld, Phys. Rev. Fluids **3,** 074101 (2018).

[5] C. Pedersen, J. F. Niven, T. Salez, K. Dalnoki-Veress, and A. Carlson, Phys. Rev. Fluids **4,** 124003 (2019).

[6] J. R. Lister, D. J. Skinner, and T. M. J. Large, J. Fluid Mech. **868,** 119 (2019).

[7] G. Peng and J. Lister, J. Fluid Mech. **905,** A30 (2020).

[8] M. Berhanu, A. Guérin, S. Courrech du Pont, F. Raoult, R. Perrier, and C. Michaut, Phys. Rev. E **99,** 043102 (2019).

[9] A. Carlson and L. Mahadevan, PLoS Comput. Biol. **11,** 1 (2015).

[10] S. Poulain, A. Carlson, S. Mandre, and L. Mahadevan, J. Fluid Mech. **947,** A16 (2022).

[11] D. Pihler-Puzović, A. Juel, G. G. Peng, J. R. Lister, and M. Heil, J. Fluid Mech. **784,** 487 (2015).

[12] G. G. Peng, D. Pihler-Puzović, A. Juel, M. Heil, and J. R. Lister, J. Fluid Mech. **784,** 512 (2015).

[13] D. Pihler-Puzović, G. G. Peng, J. R. Lister, M. Heil, and A. Juel, J. Fluid Mech. **849,** 163 (2018).

[14] J. R. Lister and R. C. Kerr, J. Geophys. Res. **96,** 10049 (1991).

[15] C. Michaut, J. Geophys. Res. **116,** B05205 (2011).

[16] A. P. Bunger and A. R. Cruden, J. Geophys. Res. **116,** B02203 (2011).

[17] A. Carlson, J. Fluid Mech. **846,** 1076 (2018).

[18] J. Eggers, J. R. Lister, and H. A. Stone, J. Fluid Mech. **401,** 293 (1999).

[19] L. Duchemin, J. Eggers, and C. Josserand, J. Fluid Mech. **487,** 167 (2003).

[20] W. D. Ristenpart, P. M. McCalla, R. V. Roy, and H. A. Stone, Phys. Rev. Lett. **97,** 064501 (2006).

[21] J. F. Hernández-Sánchez, L. A. Lubbers, A. Eddi, and J. H. Snoeijer, Phys. Rev. Lett. **109,** 184502 (2012).

[22] V. R. Kern, T. Sæter, and A. Carlson, Phys. Rev. Fluids **7,** L081601 (2022).

[23] P. J. Dekker, M. A. Hack, W. Tewes, C. Datt, A. Bouillant, and J. H. Snoeijer, Phys. Rev. Lett. **128,** 028004 (2022).

[24] P. R. Kaneelil, A. A. Pahlavan, N. Xue, and H. A. Stone, Phys. Rev. Lett. **129,** 144501 (2022).

[25] C. Coulais, J. T. B. Overvelde, L. A. Lubbers, K. Bertoldi, and M. van Hecke, Phys. Rev. Lett. **115,** 044301 (2015).

[26] See Supplemental Material at http://link.aps.org/supplemental/10.1103/PhysRevLett.132.074001 for additional information about the experiments and numerical data. It is show how the scaling of the experiments are sensitive to the choice of contact time. Additional numerical simulations show the effect of bumps of different size, the pre-wetted layer and how gravity affects the curvature estimation.

[27] A. Oron, S. H. Davis, and S. G. Bankoff, Rev. Mod. Phys. **69,** 931 (1997).

[28] R. V. Craster and O. K. Matar, Rev. Mod. Phys. **81,** 1131 (2009).

[29] C. Pedersen, T. Salez, and A. Carlson, Proc. R. Soc. A **477,** 20210354 (2021).

[30] G. I. Barenblatt, *Scaling, Self-similarity, and Intermediate Asymptotics: Dimensional Analysis and Intermediate Asymptotics*, Cambridge Texts in Applied Mathematics (Cambridge University Press, Cambridge, England, 1996).

[31] R. G. Iagar and A. Sánchez, Nonlinearity **35,** 3385 (2022).